Experimental Study on Flow Condensation of Low Global Warming Potential Refrigerants in a Micro-fin Aluminum Tube

Yifeng HU[1*], Samuel F. YANA MOTTA[1], Saad A. JAJJA[2], Cheng-Min YANG[1], Brian A. FRICKE[1], Kashif Nawaz[1]

1. Buildings and Transportation Science Division, Oak Ridge National Laboratory, Oak Ridge, TN37830, USA

2. School of Mechanical and Manufacturing Engineering (SMME), National University of Sciences and Technology (NUST), Islamabad 44000, Pakistan

* Corresponding Author

ABSTRACT

This study investigates the dynamic shifts in refrigerant technologies driven by environmental regulations, particularly emphasizing low global warming potential (GWP). Moreover, there is a rising trend in the adoption of aluminum tubes with internal axial micro-fin structures in heat exchangers to reduce costs. The research focuses on the condensation process within an expanded axial micro-fin aluminum tube with a 5.96 mm fin-tip diameter. Various refrigerants are analyzed, including both single compounds (R-32, R-1234yf, R-1234ze(E)) and zeotropic mixtures (R-454B, R-454C, R-455A). Experimental procedures cover a range of condensation temperatures (35~45 °C), reduced pressures (0.21~0.55), and mass fluxes (150~350 kg/(m² s)), providing crucial data on heat transfer coefficients (HTC) and frictional pressure gradient (FPG). This data is particularly significant for high-glide refrigerants and is instrumental in the design of advanced air conditioning and refrigeration systems aimed at mitigating global warming.

1. INTRODUCTION

The US Congress, through the American Innovation and Manufacturing Act, has authorized the Environmental Protection Agency (EPA) to reduce US production and consumption of high-global-warming-potential (GWP) hydrofluorocarbons (HFCs) by 85% by 2036 (EPA, 2023). In parallel efforts, several Western European countries have commenced the initial phase of phasing out high GWP HFCs to combat global warming (Nair, 2021).

Within the domain of air conditioning and refrigeration, prominent refrigerants such as R-410A (GWP = 2,088), R-134A (GWP = 1,430), and R-404A (GWP = 3,922) are widely utilized. In response to imperative greenhouse gas reduction targets, the chemical industry is actively investigating a spectrum of alternatives characterized by diminished Global Warming Potentials (GWPs). Immediate replacements for R-410A include R-32 (GWP = 675) and R-454B (GWP = 466), with the latter constituted by a blend comprising 68.9% R-32 and 31.1% R-1234yf (GWP = 4). Envisaging longer-term strategies, R-454C (GWP = 148), comprising 21.5% R-32 and 78.5% R-1234yf, is projected

to supplant both R-410A and R-404A. Another prospective solution, R-455A (GWP = 148), composed of 21.5% R-32, 75.5% R-1234yf, and 3% CO2, embodies GWPs below the 150 thresholds. Additionally, R-1234yf and R-1234ze(E) (GWP = 6) are being deliberated as enduring alternatives to replace R-134A.

Table 1: Prior studies on refrigerant flow condensation in micro-fin tubes**.**

Author (year)	**Refrigerants***	**D_i (mm)**	**β (°)**	**T_{Sat} (°C)**	**G (kg/m²s)**
Torikoshi and Ebisu (1993, 1994)	R-22, R-32, R-134a, R-32/R-134a	6.4	18	50	143–569
Kedzierski and Goncalves (1997), Choi et al. (1999)	R-32, R-125, R-410A, R-134a	8.92	18	22–51	85–500
Kondou et al. (2014a, 2015)	R-744/R-32/R-1234ze(E),	4.94	20	40	150–400
	R-32/R-1234ze(E)				
Kondou et al. (2014b)	R-134a, R-1234ze(E), R-1234ze(Z)	4.94	20	65	150–400
Diani et al. (2017)	R-1234yf	3.4	18	30/40	100–1,000
Diani et al. (2018a)	R-134a, R-1234yf,	2.4	7	30/40	300–1,000
	R-1234ze(E)				
Diani et al. (2018b)	R-134a, R-1234ze(E)	3.4	18	30/40	100–1,000
Hirose et al. (2018)	R-32, R-152a, R-410A	3.48	17	35	100–400
Hirose et al. (2019)	R-1234ze(E)	4.84	12–25	50	50–400
Kondou (2019)	R-1123/R-32	3	18	40	200–400
Bashar et al (2020)	R-1234yf	2.14	10	20/30	50–200
Diani and Rossetto (2020)	R-513A	2.5	7	30/40	200–1,000
Diani et al. (2020)	R-513A	3.4	18	30/40	100–1,000
Karageorgis (2021)	R-513A	8.92	15–30	35	100–440
Kim and Kim (2021)	R-448A, R-449A, R-455A, R-454C	6.3	18	45	80–400
Longo et al. (2021)	R-32, R-410A	4.2	18	29.8–40.1	98–605
Mainil et al. (2022)	R-1234yf	3	10	20/30	50–300
Irannezhad et al. (2023)	R-450A, R-454B	4.28	30	30/40	75-400
Irannezhad et al. (2024)	R-1234ze(E)	4.28	30	30/40	100-600
Lu et al. (2024)	R513A	11.8	18	33/35/38/40	40-210
		8.52	18	33/35/38/41	90-270
Ubudiyah et al. (2024)	R-32, R-1234f	3.18	10	20/30	50-200
Zhang et al. (2024)	R513A	8.8/11.9	18	35/38/40	50-250

* Low GWP refrigerants are denoted by underline text.

Previous research conducted by Jajja et al. (2022, 2023) delved into refrigerant flow condensation employing smooth copper tubing (for R-32 and R-454B) and smooth aluminum tubing (for R-32, R-454B, and R-454C). The investigation

uncovered discrepancies in heat transfer performance predictions for aluminum tubes by existing models. Additionally, it was noted that the temperature glide of refrigerant mixtures notably impacts the precision of these predictions.

Prior research did not examine the condensation heat transfer characteristics of these refrigerants using expanded micro-fin aluminum tubes. However, Yang and Hrnjak (2018) conducted a study on the flow boiling behavior of R-410A using expanded micro-fin aluminum tubes. Their findings revealed a 24% reduction in fin height and a 6.3% increase in outer diameter resulting from the expansion process. This suggests a notable potential difference in heat transfer performance between expanded and unexpanded tubes. Previous studies, as detailed in Table 1, primarily focused on flow condensation within unexpanded copper micro-fin tubes. Consequently, existing data may not accurately reflect heat transfer in expanded tubes, which could lead to inaccuracies in heat exchanger design. Furthermore, current models for condensation heat transfer are largely based on data from unexpanded copper tubes with spiral helix angles greater than 0° (ranging from 7º to 30°, as shown in Table 1). Therefore, it is crucial to assess the accuracy of these models using new data obtained for expanded tubes. Additionally, it is important to note that the flow condensation heat transfer behavior of aluminum tubes may differ from that of copper tubes due to differences in thermal conductivity. Copper tubes have approximately twice the thermal conductivity of aluminum tubes, resulting in distinct flow condensation profiles. Given the predominant focus on copper tubes in existing studies, there is a clear need to expand our understanding by investigating the condensation performance of these refrigerants in expanded micro-fin aluminum tubes. This is essential for improving the accuracy of heat exchanger design and evaluating the suitability of existing models.

Consequently, this study aims to address these gaps through experimental investigation. Six low GWP refrigerants—namely, R-32, R-454B, R-454C, R-455A, R 1234yf, and R-1234ze(E)—have been chosen for scrutiny. The research explores condensation heat transfer and frictional pressure drop of these refrigerants utilizing an axial micro-fin expanded aluminum tube with a fin tip diameter of 5.96 mm. Experimental parameters encompass condensation saturation temperatures ranging from 40 °C to 50 °C, reduced pressures ranging from 0.21 to 0.55, and mass fluxes ranging from 150 kg/(m² s) to 350 kg/(m2 s).

2. EXPERIMENTAL SETUP

2.1 Description of the Tested Systems

The experimental setup, depicted in Figure 1 , encompasses three primary loops: refrigerant, cooling water, and chiller water. To initiate the process, the refrigerant undergoes heating within a tube-in-tube heat exchanger, transitioning into superheated vapor. The outer tube of this exchanger facilitates refrigerant flow, while the inner tube accommodates electrical heaters with a total capacity of 10.2 kW. Maintaining a consistent inlet refrigerant pressure at the test section is ensured through a piston-cylinder accumulator charged with nitrogen, allowing for volume adjustments by injecting or releasing nitrogen. Visual inspection of the refrigerant's states—vapor at the inlet and liquid at the exit—is facilitated by two sight glasses, positioned at each end of the test section. Cooling water, crucial for the condensation test section, is supplied via a plate heat exchanger and a chiller, ensuring a constant flow rate and supply temperature throughout all subsequent tests. Post test section, the refrigerant undergoes further subcooling through a tube-in-tube post cooler, utilizing the same chiller's cooling source. Finally, the subcooled refrigerant completes its loop by passing through the refrigerant pump and a Coriolis flow meter. The inner diameter at the fin tip for the tested micro-finned tube is 5.96 mm, with an outer diameter of 7.59 mm. There are 54 fins, each one is 0.25 mm high and 0.21 width. Both the helix and apex angles are 0◦. Its equivalent diameter and hydraulic diameter are 6.17 mm and 2.53 mm, respectively. The relative roughness is calculated as 0.006864 by using the equation proposed by Cavallini et al. (1999). Table 2 presents the experimental uncertainties associated with both sensors and measured parameters.

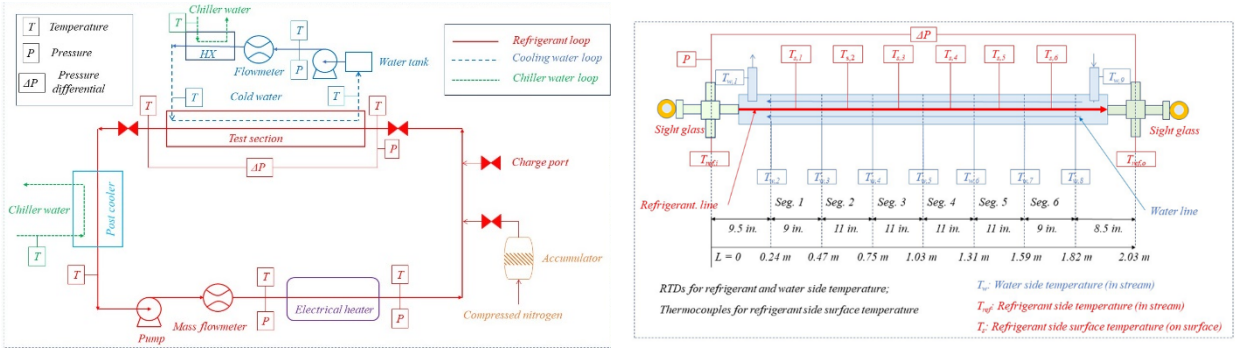

Figure 1: Schematic diagram of experimental setup and test section

Table 2: Measurement uncertainties (Hu et al., 2024)

Variable	**Uncertainty**
Refrigerant flow rate, $\dot{m}_{ref}$(kg/hr)	3.4
Water flow rate (gpm)	0.022
Refrigerant pressure, P_{ref} (kPa)	7.72
Refrigerant pressure differential, ΔP_{ref} (kPa)	0.017
Refrigerant surface temperature, T_s (°C)	0.5
Calibrated RTD temperature sensor (°C)	0.07
Water pressure, P_w (kPa)	7.55
Mass flux, G (kg/m²·s)	31.4
Heat transfer coefficient, HTC (kW/m²·K)	0.145-0.435
Quality, x (-)	2.2%-14.6%
Two-phase frictional pressure drop, ΔP_{tp} (kPa)	0.049-0.165
Frictional pressure gradient, dp/dz (kPa/m)	0.317-1.424

2.2 Test Conditions and Matrix

Table 3 delineates the test conditions applied to the six refrigerants. It is pertinent to highlight that testing at mass flux values of 300 kg/(m²·s) and 350 kg/(m²·s) at a condensation temperature of 40 °C was omitted for R-32, R-454B, R-454C, and R455A due to incomplete condensation, which was verified through visual inspection using the exit sight glass. Furthermore, for refrigerant mixtures R-454B, R-454C, and R-455A, characterized by temperature glide, the condensation saturation temperature is determined as the mean value between the dew and bubble temperatures. This methodology ensures experimental consistency by maintaining uniform condensation temperatures across all refrigerants. The refrigerant superheat at the inlet of the test section is regulated within a range of 10°C to 20°C to ensure that the incoming refrigerant is in a vapor state. Before data collection begins, a visual check of the sight glass at the inlet of the test section is conducted to verify the superheated condition.

Table 3: Test matrix

T_{cond} (°C)	Mass flux, G (kg/(m²·s))
40	150, 250, 300*, 350*
45	150, 250, 300, 350
50	150, 250, 300, 350

* Not tested for R-32, R-454B, R-454C, and R455A

2.3 Data reduction

The specific enthalpy of the refrigerant at the inlet of the test section can be determined through the following method:

$$h_{ref,i} = f\left(P_{ref,i}, T_{ref,i}\right) \tag{1}$$

where $P_{ref,I}$ represents the absolute pressure of the refrigerant at the inlet, and $T_{ref,i}$ denotes the temperature of the refrigerant at the inlet. Through a comprehensive energy balance assessment on both the water and refrigerant sides, it becomes viable to determine the specific enthalpy of the refrigerant at the outlet of each segment within the test section. This enthalpy value also serves as the inlet enthalpy for the subsequent segment. As a result, the specific enthalpy of the refrigerant at the inlet of each segment can be derived utilizing the provided equation:

$$h_{ref,i,j} = h_{ref,i,j-1} - \frac{\dot{m}_w(h_{w,j} - h_{w,j+1})}{\dot{m}_{ref}} \tag{2}$$

Where the variable j ranges from 2 to 7, with j=7 representing the exit of segment 6. $\dot{m}_w$ denotes the mass flow rate of cooling water, while $h_{w,j}$ and $h_{w,j+1}$ represent the specific enthalpy of the cooling water at each respective location. The refrigerant pressure at the inlet of each segment within the test section is determined through linear interpolation, utilizing the inlet absolute pressure and the pressure drop, according to the following method:

$$P_{ref,i,j} = P_{ref,i} - \frac{L_j}{L_{total}}\Delta P \tag{3}$$

where L_j represents the position of the segment, L_{total} is the total length of the test section, ΔP signifies the total pressure drop across the test section, and j varies from 1 to 7. The specific enthalpy and absolute pressure within each test segment are calculated as the average values of the inlet and outlet properties.

$$h_{ref,j} = \frac{h_{ref,i,j} + h_{ref,i,j+1}}{2} \tag{4}$$

$$P_{ref,j} = \frac{P_{ref,i,j} + P_{ref,i,j+1}}{2} \tag{5}$$

where j ranges from 1 to 6. The quality and temperature of the refrigerant in each segment can subsequently be determined based on these two properties by Eqs. 2 and 3. The total heat transfer in each segment is computed based on the water side:

$$Q_{cond,j} = \dot{m}_w(h_{w,j+1} - h_{w,j+2}) \tag{6}$$

where j ranges from 1 to 6. The refrigerant inner surface temperature can be determined from the outer surface temperature using the heat conduction equation:

$$T_{ref,s,\,i,j} = T_{ref,s,\,o,j} + Q_{cond,j} \cdot \left(\frac{ln\left(\frac{D_o}{D_e}\right)}{2 \cdot \pi \cdot L_{seg,j} \cdot \lambda_{tube}} \right) \tag{7}$$

The determination of the refrigerant's inner and outer surface temperatures, represented respectively as $T_{ref,s,\,i,j}$ and $T_{ref,s,\,o,j}$, is governed by the heat conduction equation. D_o and D_e are outer and equivalent diameters, $L_{seg,j}$ denoting the length of each segment, and λ_{tube} indicating the thermal conductivity of the aluminum tube. The heat transfer coefficient (HTC) in each segment can be determined using the following equation:

$$HTC_j = \frac{Q_{cond,j}}{\pi \cdot D_e \cdot L_{seg,j}\left(T_{sat,j} - T_{ref,s,\,i,j}\right)} \tag{8}$$

where $T_{sat,j}$ represents the temperature calculated based on the two properties determined by Eqs. 2 and 3. To enhance our comprehension of the heat transfer degradation of these mixtures, we formulated the following equation:

$$DF = \left(\sum_{j=1}^{n} y_j HTC_{j,exp} - HTC_{mix,\,exp}\right) \Big/ \sum_{j=1}^{n} y_j HTC_{j,exp} \tag{9}$$

where DF denotes the degradation factor, y_j represents the molar fraction of the individual component in the mixture, $HTC_{j,exp}$ signifies the experimental HTC of the individual component, and $HTC_{mix,exp}$ indicates the experimental HTC of the refrigerant mixture. Thus, our objective is to compare the experimental HTCs of the mixtures with the linear correlation of the individual HTCs. As we did not measure the HTC for CO_2 in this study, we have disregarded its impact. This is justifiable because the amount of CO2 in R-455A is only 3%, making its influence minimal in the molar calculation.

The total pressure drop (ΔP_{total}) across the test section is experimentally measured. As depicted in Eq.10. it encompasses several components: (1) sudden contraction and expansion losses (ΔP_{min}) at the inlet and exit of the test section, (2) single-phase frictional loss ($\Delta P_{fri,sp}$) occurring in both superheated vapor and subcooled liquid sections, (3) two-phase frictional drop ($\Delta P_{fri,tp}$), and (4) pressure change resulting from fluid deceleration (ΔP_{dec})

$$\Delta P_{total} = \Delta P_{fri,\,sp} + \Delta P_{fri,\,tp} + \Delta P_{min} - \Delta P_{dec} \tag{10}$$

To compute the pressure loss in each phase of the refrigerant fluid, it is crucial to determine the cutoff points of saturated vapor (x =1) and saturation liquid (x=0). Since the quality of the refrigerant has been determined at the inlet of each segment and at the exit of the last segment, we utilize a second-order polynomial method to identify these cut-points. To ascertain the pressure drop in the single-phase regions, we employed the established method proposed by Churchill (1977), as detailed in **Table 4**. Since the relative roughness (ε) is utilized, the diameter employed in the calculation of the frictional pressure drop is the equivalent diameter rather than the hydraulic diameter.

Table 4: Sing-phase pressure drop calculation method (Churchill, 1977)

Pressure drop	Equations
$\Delta P_{fri,\,sp} = \Delta P_{fri,\,G} + \Delta P_{fri,L}$	$\Delta P_{fri,sp} = f_{sp} \cdot \frac{L_{sp}}{d_e} \cdot \frac{U_{sp}^2}{2} \cdot \rho_{sp}$ $f_{sp} = 8 \cdot \left(\left(\frac{8}{Re_{sp}}\right)^{12} + \left(\theta_{sp,1} + \theta_{sp,2}\right)^{-1.5}\right)^{\frac{1}{12}};\ Re_{sp} = \frac{G \cdot D_e}{\mu_{sp}}$ $\theta_{sp,1} = \left(2.457 \cdot ln\left(\left(\left(\frac{7}{Re_{sp}}\right)^{0.9} + 0.27 \cdot \varepsilon\right)^{-1}\right)\right)^{16};\theta_{sp,2} = \left(\frac{37530}{Re_{sp}}\right)^{16}$
$\Delta P_{min} = \Delta P_{SC} + \Delta P_{SE}$	$\Delta P_{SC} = K_{SC} \cdot \frac{U_{ref,i}^2}{2} \cdot \rho_{ref,i};\ \Delta P_{SE} = K_{SE} \cdot \frac{U_{ref,o}^2}{2} \cdot \rho_{ref,o}$ $K_{SC} = 0.5 \cdot \left(1 - \left(\frac{D_e}{D_f}\right)^2\right);\ K_{SE} = \left(1 - \left(\frac{D_e}{D_f}\right)^2\right)^2$
$\Delta P_{dec} = G \cdot (U_G - U_L)$	$U_G = \frac{G}{\rho_G};U_L = \frac{G}{\rho_L};$

3. RESULTS AND DISCUSSION

Figure 2 presents an example of HTC as a function of mass flux at different qualities at the condensation temperature of 45 °C. In real-world scenarios concerning heat exchanger design, thermal engineers commonly employ the HTC within a defined mass flux range, typically with vapor quality spanning from 0.3 to 0.8, especially in situations where annular flow predominates. Therefore, the data with the quality above 0.5 for R-32, R-454B, R-454C, and R-455A and with the quality above 0.3 for R-1234yf and R-1234ze(E) are selected for further analysis.

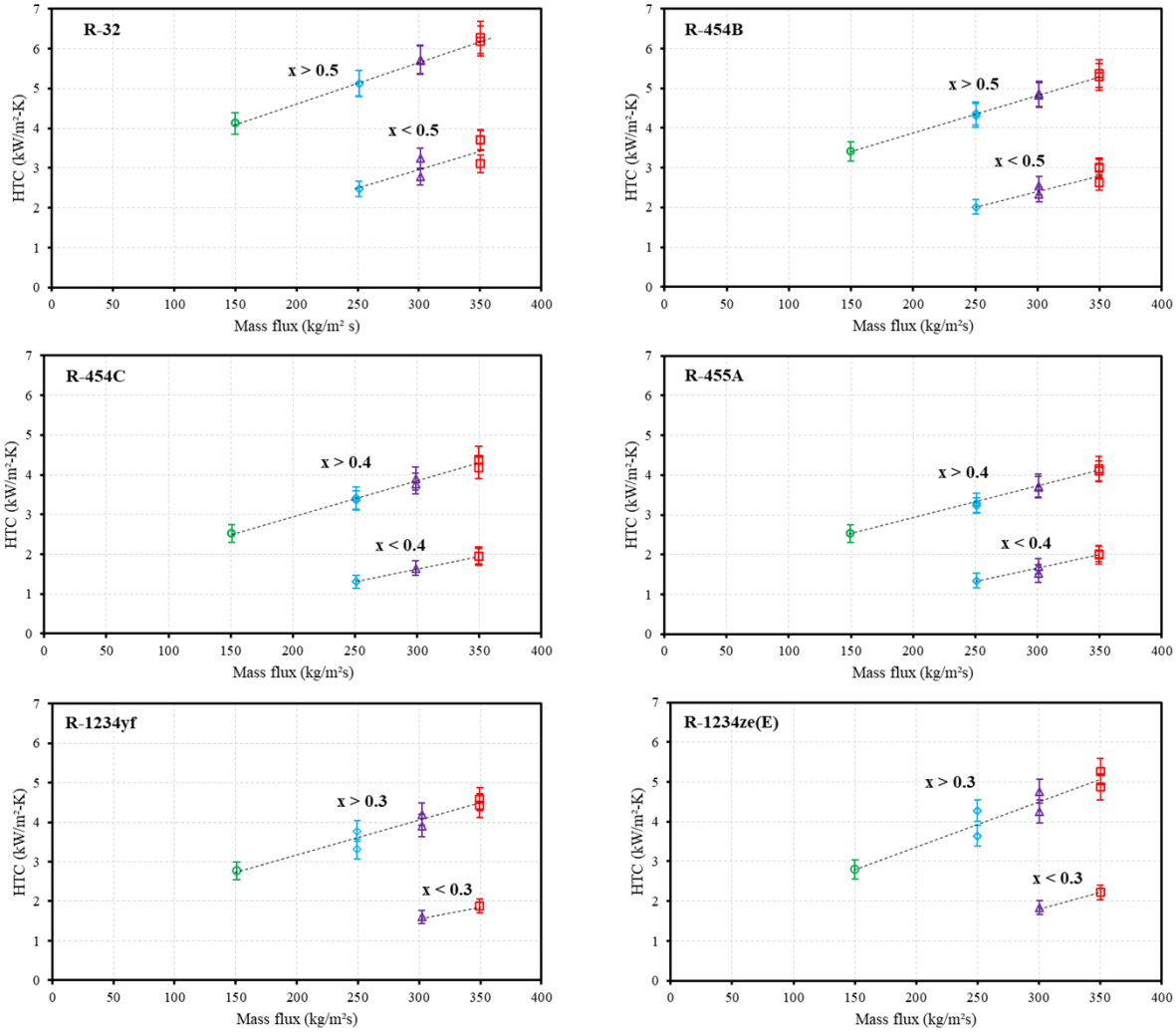

Figure 2: HTC vs. G at condensation temperature of 45°C

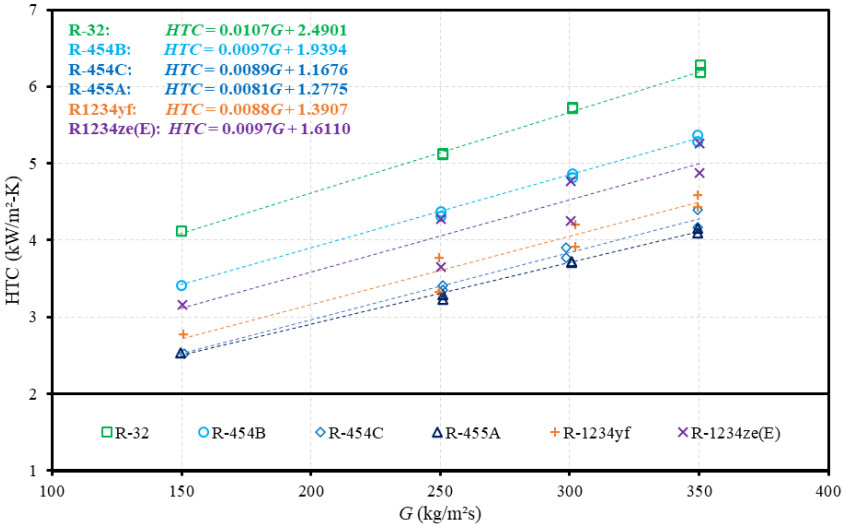

Figure 3: HTC vs. G at higher vapor qualities (0.3-0.9)

Based on the regressed equations, the degradation factor was analyzed for three refrigerant mixtures across different mass flux levels. It was observed that heat transfer degradation tends to escalate with higher-glide blends. Consequently, the blend with the highest glide (R-455A) displayed a more pronounced degradation, ranging from 25% to 30%, while the blend with the lowest glide (R-454B) demonstrated a degradation between 11% and 14%. This underscores the correlation between glide and heat transfer degradation.

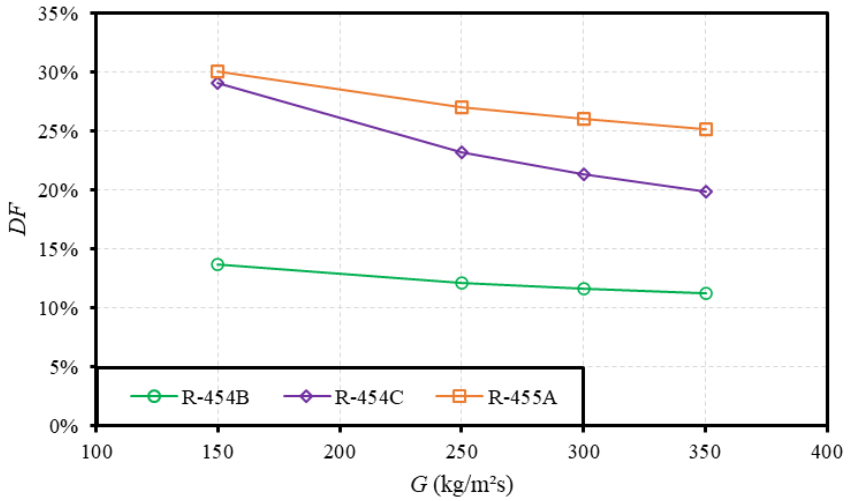

Figure 4: Degradation factor of HTC for three refrigerant mixtures

Figure 5 illustrates the pressure drop patterns associated with mass flux for each refrigerant at a condensation temperature of 45°C and HTC comparisons among these refrigerants using equivalent saturation temperature drop method. To facilitate a relevant comparison across the different refrigerants, maintaining a consistent saturation temperature drop is crucial. In this study, the average of dew and bubble temperatures is utilized as the condensation saturation temperature for refrigerant mixtures. To use an equivalent drop of the saturation temperature for HTC comparisons among these refrigerants, extrapolating frictional pressure gradient is required for R-1234yf and R-1234ze (E).

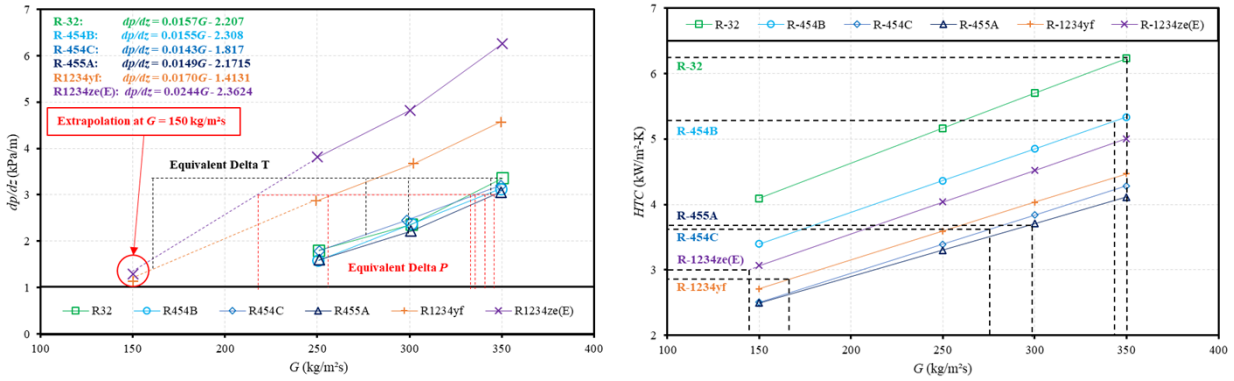

Figure 5: FPG vs. G at condensation temperature of 45 °C and HTC using equivalent saturation temperature drop

When considering an equivalent condensation saturation temperature drop, it becomes apparent that higher-pressure refrigerants can accommodate greater absolute drops in pressure. Consequently, R-32 can be engineered with a mass flux close to 350 kg/(m2·s), while lower-pressure fluids such as R-1234yf and R-1234ze(E) should ideally utilize a mass flux around 150 kg/(m2·s). This observation implies that the latter refrigerants may necessitate larger heat exchangers with more circuits compared to high-pressure refrigerants like R-32 or others such as R-454B, R-454C, and R-455A. This consideration underscores the importance of designing heat exchangers that can accommodate the specific characteristics and requirements of different refrigerants, promoting inclusivity in design considerations across various refrigerant types.

4. CONCLUSIONS

Experiments on condensation were conducted for R-32, R-454B, R-454C, R-455A, R-1234yf, and R-1234ze(E) using an expanded axial micro-fin aluminum tube. The following conclusions can be drawn:

- Heat transfer degradation varies with refrigerant glide, with high-glide blends experiencing up to 30% degradation due to internal mass transfer resistance and property non-linearity.
- Simultaneous analysis of pressure drops and HTC aids in comparing refrigerants for heat exchanger sizing, providing valuable insights for HVAC engineers.
- The study highlights the need for improved models to address heat transfer degradation in zeotropic mixtures, especially for new low GWP refrigerants, along with further research on different heat exchanger geometries and system components.

NOMENCLATURE

FPG	frictional pressure gradient	D	diameter	T	temperature
HTC	heat transfer coefficient	Δ	difference	P	pressure
DF	degradation factor	G	mass flux	U	velocity
GWP	global warming potential	h	specific enthalpy	x	quality
β	helix angle	Q	heat transfer rate	y	mole composition

REFERENCES

Bashar, M.K., Nakamura, K., Kariya, K., Miyara, A., 2020. Condensation heat transfer of R1234yf in a small diameter smooth and microfin tube and development of correlation. *Int. J. of Refrig., 120:* 331–339

Cavallini, Del Col, D., Doretti, l., Longo, G.A., L.A. Rossetto, L.A., 1999. A new computational procedure for heat transfer and pressure drop during refrigerant condensation inside enhanced tubes. *J. Enhanc. Heat Trans., 6:* 441–456.

Choi, J.Y., Kedzierski, M.A., Domanski, P.A., 1999. *A generalized pressure drop correlation for evaporation and condensation of alternative refrigerants in smooth and micro-fin tubes*. NISTIR 6333, U.S. Dept. Commerce.

Churchill, S.W., 1977. Friction-factor equation spans all fluid flow regimes, *Chem. Eng., 84* (24): 91–92.

Diani, A., Brunello, P., Rossetto, L., 2020. R513A condensation heat transfer inside tubes: Microfin tube vs. smooth tube. Int. *J. Heat Mass Trans. 152:* 119472

Diani, A., Campanale, M., Cavallini, A., Rossetto, L., 2018a. Low GWP refrigerants condensation inside a 2.4 mm ID microfin tube. *Int. J. of Refrig. 86:* 312–321.

Diani, A., Campanale, M., Rossetto, L., 2018b. Experimental study on heat transfer condensation of R1234ze(E) and R134a inside a 4.0 mm OD horizontal microfin tube. *Int. J. Heat Mass Trans., 126:* 1316–1325

Diani, A., Cavallini, A., Rossetto, L., 2017. R1234yf condensation inside a 3.4 mm ID horizontal microfin tube. *Int. J. of Refrig., 75:* 178–189.

Diani, A., Rossetto, L., 2020. Condensation of an azeotropic mixture inside 2.5 mm ID minitubes. Fluids, 5: 171.

El Hajal, J., Thome, J. R., Cavallini, A., 2003. Condensation in horizontal tubes, part 1: Two-phase flow pattern map. *Int. J. Heat Mass Trans., 46* (18): 3349–3363.

EPA, 2023. *HFC Allowance Allocation and Reporting*. U.S. Environmental Protection Agency.

Hirose, M., Ichinose, J., Inoue, N., 2018. Development of the general correlation for condensation heat transfer and pressure drop inside horizontal 4 mm small-diameter smooth and microfin tubes. *Int. J. of Refrig., 90:* 238–248.

Hirose, M., Jige, D., Inoue, N., 2019. Optimum fin geometries on condensation heat transfer and pressure drop of R1234ze(E) in 4-mm outside diameter horizontal microfin tubes. *Sci. Technol. Built Environ., (25)* 10: 1271–1280.

Hu, Y., Jajja, S. A., Yang, C. M., Motta, S. F. Y., Fricke, B. A., & Nawaz, K., 2024. In tube condensation of low global warming potential refrigerants in an axial micro-fin aluminum tube. *Int. J. of Refrig., 161:* 221-241.

Irannezhad, N., Rossetto, L., & Diani, A. (2024). A comprehensive study with high-speed camera assisted visualizations of HFO-1234ze (E) condensation inside an enhanced tube. *Int. Comm. Heat Mass Trans.*, 150: 107203.

Irannezhad, N., Rossetto, L., & Diani, A., 2023. Flow Condensation of Low-GWP Zeotropic Mixtures Inside 5 mm OD Micro-Finned Tube. *App. Sci., 14* (1): 373.

Jajja, S.A., Fricke, B.A., Nawaz, K., 2023. Condensation heat transfer and pressure drop of low-global warming potential refrigerants in smooth aluminum tubes. *App. Therm. Eng., 237:* 121774.
Jajja, S.A., Nawaz, K., Fricke, B.A., 2022. In tube condensation heat transfer and pressure drop for R454B and R32—Potential replacements for R410A. *Int. J. of Refrig., 144:* 238–253.
Karageorgis, A., Hinopoulos, G., Kim, M.H., 2021. A comparative study on the condensation heat transfer of R-513A as an alternative to R-134a. *Machines, 9:* 114.
Kedzierski, M.A., Goncalves, J.M., 1997. *Horizontal convective condensation of alternative refrigerants within a micro-fin tube*, NISTIR 6095, U.S. Dept. Commerce.
Kim, C.H., Kim, N.H., 2021. Condensation heat transfer and pressure drop of low GWP R-404A-alternative refrigerants (R-448A, R-449A, R-455A, R-454C) in a 7.0-mm outer-diameter horizontal microfin tube. *Int. J. of Refrig., 126:* 181–194.
Kondou, C., 2019. Heat transfer and pressure drop of R1123/R32 (40/60 mass%) flow in horizontal microfin tubes during condensation and evaporation. *Sci. Technol. Built Environ., 25:* 1281–1291.
Kondou, C., Mishima, F., Koyama, S., 2015. Condensation and evaporation of R32/R1234ze (E) and R744/R32/R1234ze (E) flow in horizontal microfin tubes. *Sci. Technol. Built Environ. 21* (5): 564–577.
Kondou, C., Mishima, F., Liu, J., Koyama, S., 2014a. Condensation and evaporation of R744/R32/R1234ze (E) flow in horizontal microfin tubes. *Proceed. Int. Refrig. Air Cond. Conf.,* West Lafayette, IN. Purdue University, Paper 1448.
Kondou, C., Mishima, F., Liu, J., Koyama, S., 2014b. Condensation and evaporation of R134a, R1234ze (E) and R1234ze (Z) flow in horizontal microfin tubes at higher temperature. *Proceed. Int. Refrig. Air Cond. Conf.,* West Lafayette, IN. Purdue University, Paper 1446.
Longo, G.A., Mancin, S., Righetti, G., Zilio, C., 2021. Comparative analysis of microfin vs smooth tubes in R32 and R410A condensation. *Int. J. of Refrig., 128:* 218–231.
Lu, Z., Jiang, J., Tang, C., Tao, L., Chen, J., Zheng, Z., & Huang, L., 2024. Research on the R513A condensation heat transfer characteristics in horizontal microfin tubes. *Int. Comm. Heat Mass Trans.*, *154:* 107462.
Mainil, A.K., Sakamoto, N., Ubudiyah, H., Kariya, K., Miyara, A., 2022. Experimental study and general correlation for frictional pressure drop of two-phase flow inside microfin tubes. *Int. J. of Refrig., 144:* 342–353
NIST, *Refprop 10 - Refrigerants Properties Database*, 2022.
Nair, V. (2021). HFO refrigerants: A review of present status and future prospects. *Int. J. of Refrig., 122*: 156-170.
Torikoshi, K., Ebisu, T., 1993. Heat transfer and pressure drop characteristics of R134a, R32, and a mixture of R32/R134a inside a horizontal tube. *ASHRAE Trans., 99:* 90–96.
Torikoshi, K., Ebisu, T., 1994. In-tube heat transfer characteristics of refrigerant mixtures of R32/R134a and HFC32/125/134a. *Proceed. Int. Refrig. Conf.*, West Lafayette, IN, pp. 293–298.
Ubudiyah, H., Mainil, A. K., Kariya, K., & Miyara, A., 2024. Experimental study and general correlation for condensation heat transfer coefficient inside microfin tubes. *Int. J. of Refrig., 158:* 422-430.
Yang, C.M., Hrnjak, P., 2018. Effect of straight micro fins on heat transfer and pressure drop of R410A during evaporation in round tubes. *Int. Heat Mass Trans., 117:* 924–939.
Zhang, S., Tao, L., Huang, L., & Jin, C., 2024. Entropy generation of R513A condensation flow inside the horizontal microfin tubes. *J. Therm. Sci. Eng. App., 16:* 1-11.

ACKNOWLEDGEMENT

The US Department of Energy's Building Technologies Office funded the project, with refrigerant research samples provided by Honeywell and Chemours. Elliott Fountain assisted with rendering the condensation test section, and Brian Goins, Jeff Taylor, Brent Massey, Mike Day, Charles Pierce, and Tim Dyer supported the experimental infrastructure. Dr. Mark A. Kedzierski from NIST provided valuable comments to enhance our study.